Removal of Pb (II) from aqueous solution by using micro-spheres of *Zea mays* rachis–sodium alginate by batch and column systems

D. Gutiérrez-López, N. Flores-Alamo, M. C. Carreño-de-León and M. J. Solache-Rios

ABSTRACT

The behavior of composite beads of *Zea mays* rachis and sodium alginate (AL) for Pb (II) adsorption was studied. The *Zea mays* rachis–sodium alginate was prepared and characterized. The IR spectra showed interactions of the functional groups and the metal ions after adsorption. The kinetic data were fitted to the pseudo-first- and pseudo-second-order models, the maximum adsorption capacity was 60 mg/g for Pb (II), and the isotherm data were best adjusted to the Freundlich model, indicating that the adsorbent is heterogeneous. The thermodynamic study shows that the process is physisorption. The service time of columns increases as the height of columns increases, and this behavior was attributed to the active sites available in the columns. The initial concentration of Pb (II) had a significant effect on the breakthrough curves. As the concentration increases, the saturation time decreases. The material was regenerated four times (adsorption–desorption cycles), without a significant change in the removal efficiencies.

Key words | bioadsorption, isotherms, lead, water

D. Gutiérrez-López
N. Flores-Alamo (corresponding author)
M. C. Carreño-de-León
División de Estudios de Posgrado e Investigación,
Tecnológico Nacional de México/Instituto Tecnológico de Toluca,
Av. Instituto Tecnológico S/N, Colonia Agrícola Bellavista, C.P. 52149, Metepec, Estado de México,
México
E-mail: *nfloresa@toluca.tecnm.mx*

D. Gutiérrez-López
M. J. Solache-Rios
Departamento de Química,
Instituto Nacional de Investigaciones Nucleares,
Carretera México-Toluca S/N, La Marquesa, Ocoyoacac, Estado de México, C. P. 52750,
México

INTRODUCTION

Heavy metals are used in human activities such as in the industrial, agricultural and mining sectors. The increase of these activities and their by-products affect the entire trophic chain of the ecosystem and causes one of the main environmental problems, due to their accumulation in biotic and abiotic systems (Febrianto *et al.* 2009).

Lead is an important industrial metal which is used in the paint industry, metallurgy, mining, electrical manufacturing and munitions storage. Lead is a toxic element and may be generated by the corrosion of galvanized pipes, runoff water in urban centers and mineral stacks.

Conventional methods such as chemical precipitation, electrodeposition, and reverse osmosis for the removal of metal ions are expensive and ineffective when the concentration of heavy metals in solution is low. For this reason new inorganic adsorbents of natural origin have been studied for the removal of metals at low concentrations (Hasan *et al.* 2008). Some of these materials may be regenerated and some residues, abundant in nature, can be used (Al-Anber & Al-Anber 2008). The *Zea mays* rachis (ZMR), commonly known as corn cob, is a lignocellulosic material and has hydroxyl and carboxyl functional groups, which may interact with metal ions in aqueous solution.

Some adsorbent materials can be treated to improve their mechanical and chemical properties in order to use them in fixed bed columns for the removal of metal ions. Adsorbents based on agricultural waste have been rarely studied. Guyo *et al.* (2015) conducted studies on Pb (II) adsorption in aqueous solutions using unmodified and NaOH-modified maize stubble as adsorbent. The studies were carried out in a batch system and the maximum adsorption capacity was 19.65 mg/g for maize stubble without chemical treatment and 27.10 mg/g for the modified maize stubble. Chatterjee & Schiewer (2014) studied the

doi: 10.2166/ws.2020.107

adsorption of Cd in aqueous solutions using orange peel immobilized on calcium alginate beads as adsorbent, and the maximum adsorption capacity was 35 mg/g. Cardona Gutiérrez *et al.* (2013) studied the adsorption of Pb (II) in aqueous solutions using orange peel as adsorbent and the maximum adsorption capacity was 9.39 mg/g. Mahajan & Sud (2013) studied the biosorption of Ni (II) and Cu (II) in aqueous solutions using peanut husk immobilized on calcium alginate beads as adsorbent and it was found that the metals compete for the sorption sites. The low adsorption of Cu (II) was attributed to this behavior and the maximum sorption capacities were 30.76 and 18.16 mg/g for Ni (II) and Cu (II) respectively. Park *et al.* (2008) used banana peel immobilized on calcium alginate beads as adsorbent for the removal of total Cr from aqueous solutions and the results showed that immobilization reached adsorption percentages of 96–97%.

The main objective of this research was to evaluate the adsorption capacity of Pb (II) in aqueous solution in both batch and continuous systems using rachis *Zea mays*, supported on sodium alginate. This polymer does not require extreme reaction conditions and it is low in cost and toxicity, and easy to prepare.

METHODS

The ZMR was triturated, washed with distilled water and dried at 40 °C for 72 h. Then the material was milled and sieved (100 mesh, 0.149 mm). Sodium alginate and calcium chloride ($CaCl_2$) were used as the crosslinking agent to support the ZMR. Lead solutions were prepared from lead nitrate and distilled water.

Preparation and characterization of the composite

The adsorbent material was synthesized in a 1:4 sodium alginate and *Zea mays* rachis (AL-ZMR) ratio. Four grams of ZMR were added to 100 mL of a 1% w/w of alginate (AL) solution and the mixture was shaken until homogenized. Then the mixture was dripped with a peristaltic pump in a 0.01 M $CaCl_2$ solution with constant stirring (400 rpm), and then the mixture was left for 24 h. The beads were washed with distilled water to remove excess $CaCl_2$, until the pH of the washing solutions was equal to the distilled water.

The AL-ZMR 1:4 beads were characterized by scanning electron microscopy (SEM) to determine the morphology of the material before and after the adsorption of Pb (II) by using a JEOL JSM-590-LD microscope at 10 kV. In all cases the images were taken with a backscattered electron detector. Elementary chemical compositions of the samples were determined by energy dispersive spectroscopy (EDS, Oxford Penta FET). The functional groups present in the adsorbent were identified by Fourier transform infrared spectrophotometry (FTIR), equipped with a diamond-tipped ATR accessory (FTIR-ATR, Varian 640) at wave-number range from 4,000 to 400 cm^{-1}.

The zero-point charge (pH-zpc) was determined as follows: 0.05 g of dried pearls were placed in contact with 10 mL aliquots of 0.1 M $NaNO_3$ solution of different pH values (2–11) in continuous stirring for 24 h and at 25 °C. Then, the final pH (pH_{end}) values of the solutions were measured and a graph of ΔpH ($pH_{in} - pH_{end}$) vs pH_{in} was plotted (Hernández-Hernández *et al.* 2013).

The swelling kinetics of the AL-ZMR pearls was determined as follows: 0.05 g of dried pearls were placed in contact with distilled water in continuous stirring, the pearls were removed from the water at different times, dried with absorbent paper to remove the excess of water, weighed, and then they were returned to the container and the same procedure was repeated until the weight of the pearls was constant.

Adsorption tests in batch

Ten mL of Pb (II) solution of pH 5 and 0.05 g of dry AL-ZMR beads were left in continuous stirring by using a Heidolph thermal mixer (Unimax 2020 model) at 200 rpm. After the contact time, the solution was separated from the beads and the concentration of the Pb (II) was measured by using absorption spectrophotometry (Perkin Elmer spectrophotometer, model 31104) at 216.8 nm, and then the adsorption capacity (q_t) was determined by Equation (1) (Athar *et al.* 2013):

$$q_t = \frac{(C_0 - C_t)V}{w} \quad (1)$$

where C_0 and C_t are the initial and at time t concentrations (mg/L) respectively, V is the volume of the solution (L) and w is the weight of the AL-ZMR beads in dry base (g).

Effect of pH on the adsorption capacity of Pb (II)

Aliquots of 10 mg/L of Pb (II) at different pH (3–8) and 0.05 g of dry AL-ZMR beads were left in contact for 120 min, then the solutions were decanted and the lead was measured in each solution.

Adsorption kinetic experiments

The adsorption kinetics experiments were carried out with continuous shaking contact times of 2, 3, 5, 10, 20, 30, 60, 90 and 120 min, using a 10 mg/L solution of lead at pH 5. Experimental data were treated with the pseudo-first- (Equation (2)) and the pseudo-second-order (Equation (3)) kinetic models (Ho & McKay 1998; Pinzón-Bedoya & Vera Villamizar 2009; Vilchis 2013):

$$q_t = q_e(1 - e^{-k_1 t}) \tag{2}$$

$$q_t = \frac{k_2 q_e^2 t}{1 + k_2 q_e t} \tag{3}$$

where q_t and q_e are the adsorption capacities at time t and at equilibrium (mg/g) respectively, and k_1 (1/h) and k_2 (mg/(g·h)) are the rate constants of adsorption of the pseudo-first and the pseudo-second order.

Adsorption isotherm experiments

Solution aliquots at the optimum pH value of 5 with initial concentrations of Pb (II) between 2 and 300 mg/L and 0.05 g of dry AL-ZMR beads were left in continuous stirring (200 rpm) for 60 min and the experiments were performed at 25, 40 and 50 °C. The experimental data were adjusted to the Langmuir and Freundlich models. In the Langmuir model (Equation (4)) the absorption is limited to a single adsorbed monolayer on the adsorbent surface, which can be interpreted as a complete coating of the adsorbent surface by a maximum amount of adsorbate (monolayer limit). This type of isotherm is related to homogeneous surfaces. The Freundlich isotherm indicates that the surface is heterogeneous and the adsorption isotherms do not present a clear limit of adsorption (Equation (5)) (Wang & Chen 2009; Liu *et al.* 2010):

$$q_e = \frac{q_{max} b C_e}{1 + b C_e} \tag{4}$$

$$q_e = k_F C_e^{1/n} \tag{5}$$

where q_{max} and q_e are the maximum adsorption and equilibrium capacity respectively (mg/g), C_e is the concentration of Pb (II) at equilibrium in the aqueous solution (mg/L) and b, K_F and n are the model constants.

Thermodynamic parameters

The thermodynamic parameters were determined from the equilibrium data (isotherms). These parameters allowed the estimation of the feasibility of the process, as well as the effect of the temperature on the adsorption process (Almeida *et al.* 2009).

The Van 't Hoff equation was used to calculate the enthalpy (ΔH) and the entropy ΔS, (Equation (6)) (Roulia & Vassiliadis 2008):

$$\ln\left(\frac{q_e}{C_e}\right) = \frac{\Delta S}{R} - \frac{\Delta H}{R}\left(\frac{1}{T}\right) \tag{6}$$

where q_e is the adsorption capacity of the adsorbent material (mg/g), C_e is the concentration of Pb (II) in solution at equilibrium (mg/L), R is the universal gas constant (8.314 J/mol·K) and T is the temperature (K). Equation (7) was used to calculate Gibbs free energy (Chang 2007):

$$\Delta G = \Delta H - T * \Delta S \tag{7}$$

Continuous adsorption tests

Continuous adsorption tests were performed using a 1 cm diameter glass column packed with 0.423, 0.847 and 1.27 g of AL-ZMR beads on a dry basis (bed heights were 2, 4 and 6 cm respectively). Aqueous solutions of Pb (II)

with concentrations of 10 and 30 mg/L were fed by upflow at a rate of 3 mL/min using a peristaltic pump. The experiments were carried out at 25 °C and pH of 5. Samples were taken at different times (volumes) and the concentration of Pb (II) in the solution was measured by atomic absorption spectroscopy.

Experimental parameters for dynamic response depend on column operating parameters such as feed ion concentration (C_0, mg/L) and flow rate Q (mL/min). A breakthrough curve is usually expressed in terms of adsorbed pollutant concentration (C_{ad}) or normalized concentration defined as the ratio of effluent pollutant concentration to inlet pollutant concentration (C/C_0) as a function of time (t, min) for a given bed height (equivalent weight). The area under the breakthrough curve (A) can be obtained by integrating the adsorbed concentration (C_{ad}) versus t plot. Total adsorbed pollutant quantity (q_{total}, mg) in the column for a given feed concentration and flow rate is calculated from Equation (8) (Sankararamakrishnan *et al.* 2008):

$$q_{total} = \frac{Q \cdot A}{1000} = \frac{Q}{1000} \cdot \int_{t=0}^{t=t_{total}} C_{ad} \quad (8)$$

The total amount of pollutant passing through the column (m_{total}, mg) is calculated from Equation (9):

$$m_{total} = \frac{C_0 \cdot Q \cdot t_{total}}{1000} \quad (9)$$

The removal percentage of pollutant (column performance) with respect to flow volume can be also found from the ratio between q_{total} and m_{total} (Equation (10)):

$$Removal = \frac{q_{total}}{m_{total}} \cdot 100 \quad (10)$$

Equilibrium dye uptake (q_e, mg/g) (or column capacity) in the column is defined by Equation (11) as the total amount of dye sorbed (q_{total}) per gram of sorbent (m):

$$q_e = \frac{q_{total}}{m} \quad (11)$$

Adsorbent material regeneration

The regeneration was carried out during five adsorption–desorption cycles in the column system to determine the adsorption capacity in each cycle. A solution of 30 mg/L of Pb (II) was pumped through a fixed bed column (1 cm height) for 5 h at a flow rate of 3 mL/min. Then, a nitric acid solution at pH of 3 was passed through the bed for 2 h (3 mL/min), and the samples were taken every 10 min. After each cycle the beads were washed with distilled water to avoid changes in the operating conditions for the next regeneration cycle.

RESULTS AND DISCUSSION

Characterization of the ZMR–sodium alginate beads

The average diameter of the beads was 1.85 ± 0.2 mm. The micrographs of the Al-ZMR (Figure 1) show a rough and porous surface morphology, and these irregularities can be favorable for the process of adsorption of metal ions (Vijayalakshmi *et al.* 2017).

The EDS analysis of the beads before and after the adsorption process (Figure 2) shows the presence of C, O and Ca before the adsorption process. $CaCl_2$ was used in the synthesis of the microspheres (Ren *et al.* 2016) and the presence of minority elements like silicon (Si) is common in the ZMR, due to the transport mechanisms of nutrients in the plants (Juárez 2014). After the adsorption process, Pb (II) was found on the material surface (Vijayalakshmi *et al.* 2017) and calcium was not observed, most probably due to the ion exchange with Pb (II). This behavior suggests that the adsorbent has the potential for Pb (II) removal from aqueous solution.

The FTIR spectra (Figure 3) for ZMR without sodium alginate support (ZMR), before (Al-ZMR) and after the adsorption of Pb (II) (ZMR-AL-Pb(II)) were analyzed to identify the functional groups that interact with the Pb (II) ions. A wide band at 3,324 cm^{-1} was observed for the AL-ZMR, corresponding to OH- groups. The peak observed at 2,924 cm^{-1} describes the stretching and bending vibrations of -CH bonds, representative of the CH_2 groups. The band at 1,605 cm^{-1} corresponds to the elongation of the carbonyl

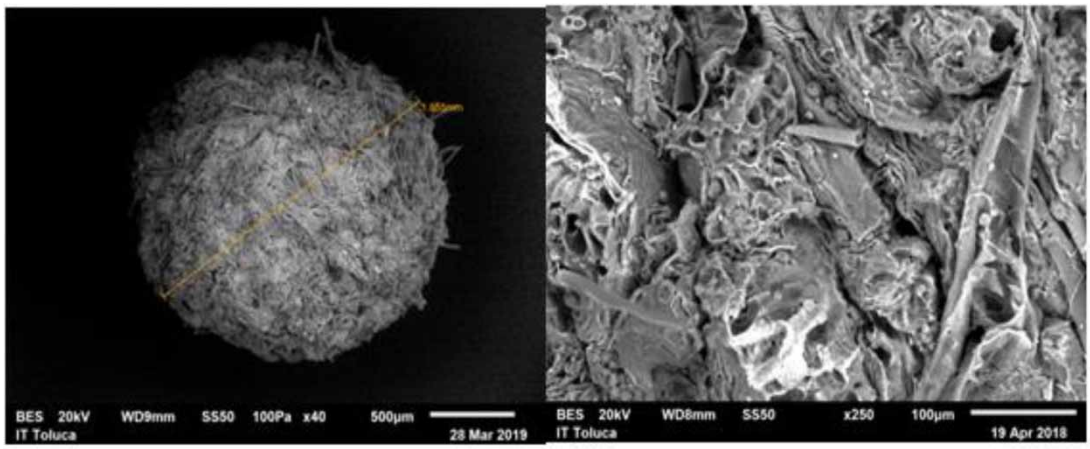

Figure 1 | SEM micrographs of AL-ZMR.

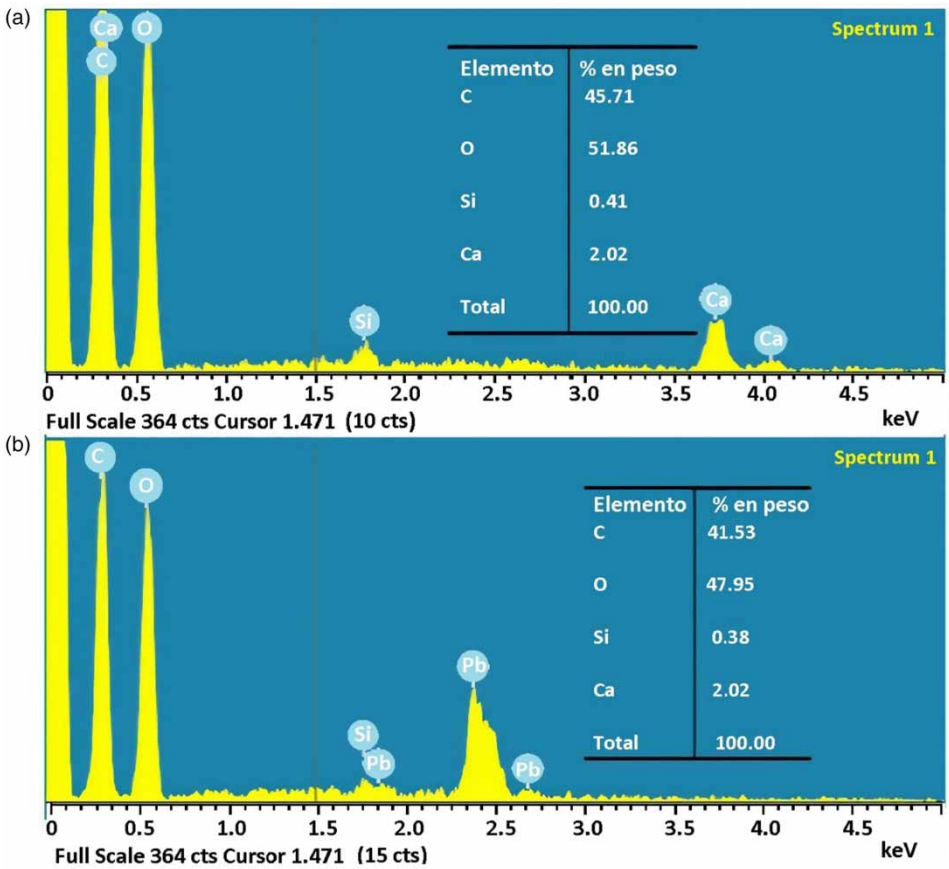

Figure 2 | EDS analysis of AL-ZMR: (a) before and (b) after the adsorption of Pb (II) ions.

(C = O) group belonging to the carboxyl group and the peak at 1,420 cm^{-1} corresponds to C-C stretching vibrations in the cyclic structure of the alginate. The band at 1,244 cm^{-1} corresponds to vibration of the ether groups which are part of glycosidic (C-O-C) bonds, and the peak at 1,026 cm^{-1} corresponds to hydroxyl groups that are

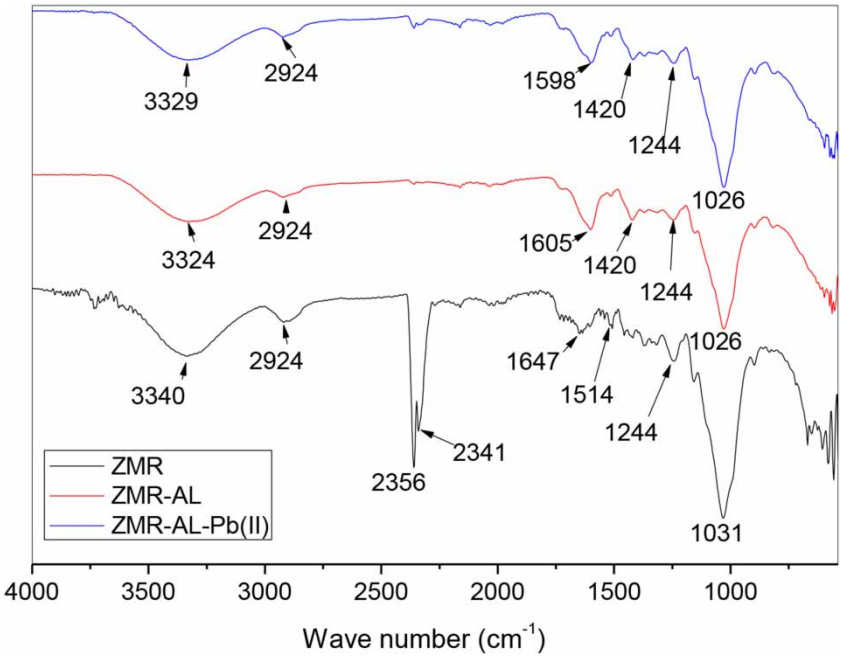

Figure 3 | FTIR spectrum of ZMR and beads of AL-ZMR before and after the adsorption process.

characteristic in cellulose structure, hemicellulose and lignin which are present in the ZMR (Tan *et al.* 2010; Guyo *et al.* 2015; Petrović *et al.* 2016).

Two bands were observed at 2,356 and 2,341 cm^{-1} in the ZMR, produced by PH (phosphine) vibrations. These bands were not observed in the pearls, perhaps as a consequence of the synthesis process. Other different displacements were observed between the ZMR-AL and the ZMR beads, which denotes a different structure once the ZMR is supported on alginate.

The band of the OH- groups shifted to 3,329 cm^{-1}, responsible for the removal of Pb (II) from solution. More evidence of interaction between the functional groups of the ZMR-AL and Pb (II) ions was the asymmetric vibrations of the C = O group which shifted from 1,605 to 1,598 cm^{-1}.

Some absorption bands coincide with other studies performed with corn ear and these bands are located at 3,287, 2,918, 1,732 and 1,420 cm^{-1}, which correspond to the groups OH^{-}, -CH, C = O and C = C respectively (Petrović *et al.* 2016), and in rachis of *Zea mays* with absorption bands at 1,022 cm^{-1} that are attributed to phenolic groups and symmetrical vibrations at 1,238 cm^{-1} belonging to the ether group (C-O-C) (Carreño de León *et al.* 2016).

The zero-point charge of the beads was found at pH of 4.6 (Figure 4). At this pH value the total net charge on the surface is zero and the number of sites with positive and negative charges is the same. Below this pH value the surface charge of the beads is positive and can adsorb negatively charged species. Above this value the surface charge of the material is negative, due to the deprotonation of some functional groups such as carboxyls and to the increase of hydroxyl ions, therefore pearls can adsorb positively charged species (Worch 2012; Amaringo Villa & Hormaza Anaguano 2013). The values corresponding to

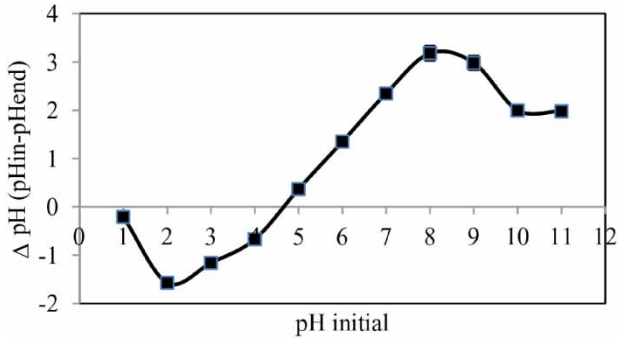

Figure 4 | Zero-point charge of AL-ZMR beads.

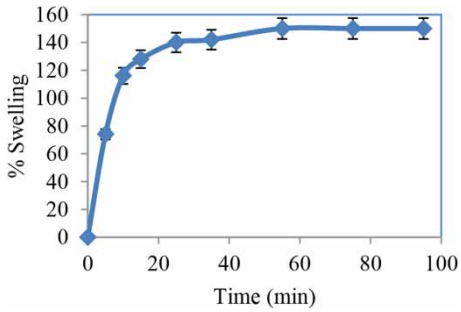

Figure 5 | Swelling of AL-ZMR pearls vs time.

the initial pH of 1, 9, 10 and 11 do not follow the trend of the other experimental values and this effect can be attributed to the change of the bed structure (Carreño de León *et al.* 2017).

The swelling kinetics of the AL-ZMR beads in water (Figure 5) showed that with respect to their initial weight (0.05 g) the pearls swelled 74% in 5 min (0.087 g) and in 10 min they doubled their initial weight (0.108 g). The maximum swelling of the beads was 150%, which was reached in 55 min (0.125 g).

Adsorption in batch

Effect of pH on the adsorption capacity of Pb (II)

The adsorption of metal ions is affected by the pH of the metal solution, since the pH affects both the adsorbent and the chemical species of the metal in the solution (Makeswari *et al.* 2016). The effect of pH on the adsorption of Pb (II) is shown in Figure 6; at pH between 3 and 6 the removal percentage is around 96.8%. The percentage decreases at pH 7 and 8, probably due to the formation of hydrolyzed species of lead (García-Rosales & Colín-Cruz 2010).

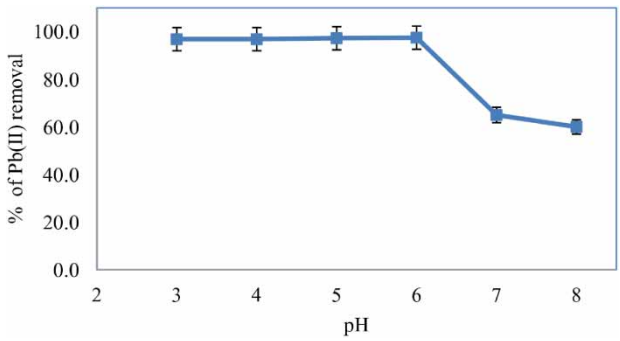

Figure 6 | Influence of pH on the removal of Pb (II).

Adsorption kinetics

The adsorption kinetics curves (Figure 7) obtained at different temperatures show that the amount of Pb (II) adsorbed by the AL-ZMR beds increases as the contact time increases, and the adsorption capacity at the equilibrium (60 min) is 2.04 mg/g at 25 °C. The equilibrium time decreased (30 min) for the experiments performed at 40 and 50 °C.

The adjustments of the experimental data to the models are shown in Figure 7. The points represent the experimental data; the solid line is the adjustment to the pseudo-first-order model (Lagergren) and the dotted line is the adjustment to the pseudo-second-order model (Ho and McKay). Table 1 shows the kinetic parameters obtained from the adjustments of the experimental data to the models. The R^2 value for the Ho and McKay equation was in all cases higher than 0.99, showing a good fitting of the experimental data to this model. In addition, the value of q_e, calculated from the pseudo-second-order model, is similar to the experimental one (q_e exp).

Adsorption isotherms

Figure 8 shows the adsorption isotherms at 25, 40 and 50 °C. The adsorption capacity increases as both the initial concentration of the metal in solution and the temperature increase.

The trend of the experimental data in the concentration range studied shows similarity with the characteristic curve of Freundlich's isotherm (a plateau was not observed), therefore, the data were adjusted only to this model and the results are shown in Figure 8 and Table 2. The points represent the experimental data and the solid lines the fittings to the Freundlich model.

The Freundlich model proposes an adsorption process that occurs in multiple layers on a heterogeneous surface, and it also assumes that the adsorption capacity depends on the concentration of the sorbate in solution. The sorption capacity increases as the concentration increases (Febrianto *et al.* 2009; Moyo *et al.* 2013).

The value of the constant K_F is related to the sorption capacity, while $1/n$ is related to the sorption intensity. A value close to the unit indicates a favorable sorption intensity (Foo & Hameed 2010; Guyo *et al.* 2015). The values of $1/n$ from the experimental data and the fitting to the

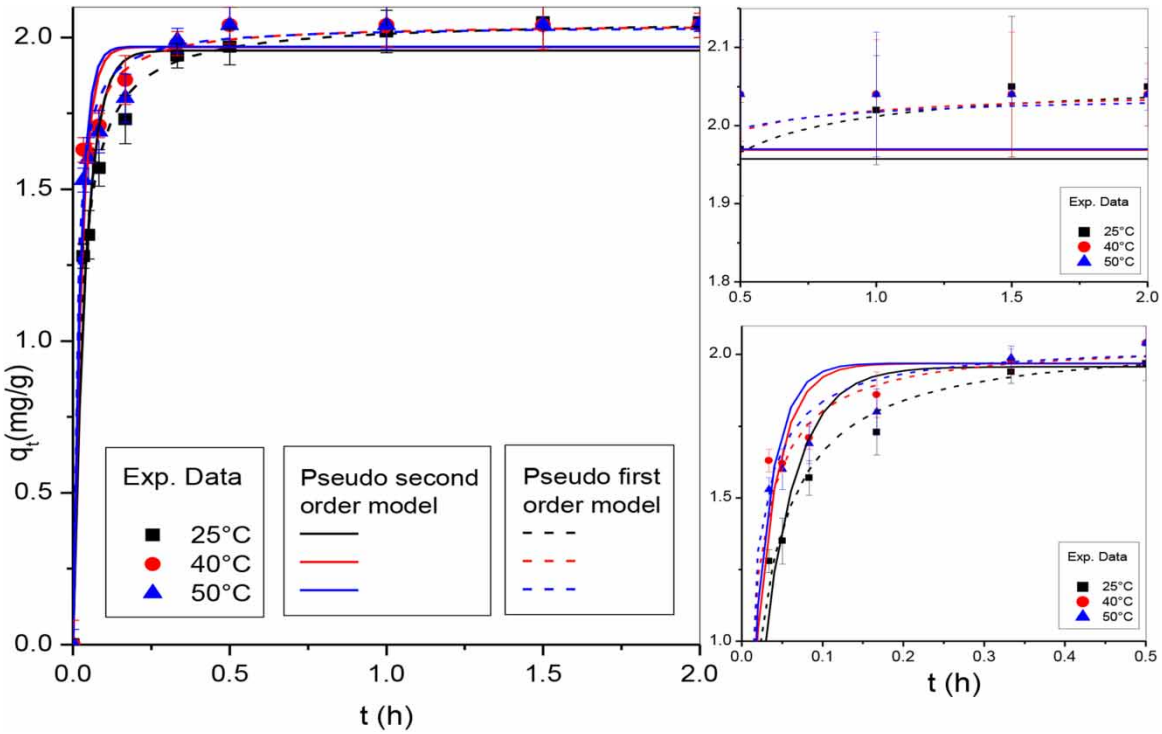

Figure 7 | Adsorption kinetics for Pb (II) by AL-ZMR at different temperatures.

Table 1 | Kinetic parameters of the adsorption of Pb (II) by AL-ZMR

	Pseudo-first-order model			Pseudo-second-order model			
T (°C)	K_1 (1/h)	q_e (mg/g)	R^2	K_2 (mg/g h)	q_e (mg/g)	R^2	q_e exp (mg/g)
25	24.83	1.95	0.964	20.22	2.06	0.995	2.05
40	42.00	1.97	0.966	44.31	2.04	0.991	2.04
50	37.24	1.97	0.966	36.34	2.04	0.992	2.04

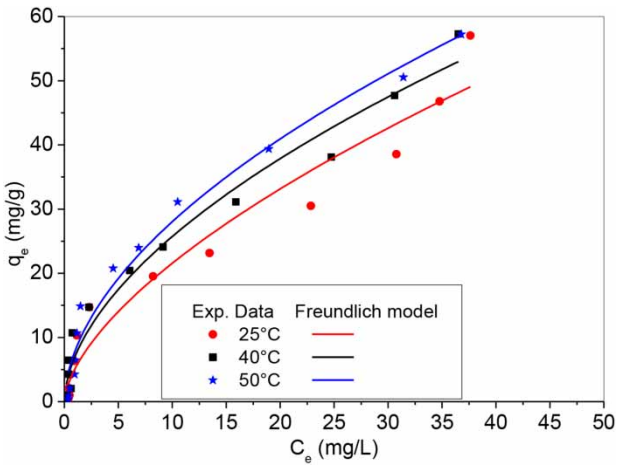

Figure 8 | Isotherms for the adsorption of Pb (II) by AL-ZMR at 25, 40 and 50 °C.

Table 2 | Parameters of the adsorption isotherms of Pb (II) by ZMR-AL

	Freundlich			
T (°C)	K_F (mg/g)(L/mg)$^{1/n}$	n	$1/n$	R^2
25	1.79	1.5	0.66	0.95
40	5.16	1.27	0.78	0.97
50	7.11	1.39	0.71	0.97

Freundlich model were from 0.66 to 0.78, and when $1/n$ values are in the range of 0 and 1 the interactions between sorbate and adsorbent are strong. Figure 8 shows that the maximum adsorption capacity of ZMR-AL for Pb (II) is >40 mg/L, which is higher than the adsorption capacities reported for other materials such as unmodified and NaOH-modified maize stubble (Guyo *et al.* 2015) and orange peel (Cardona Gutiérrez *et al.* 2013).

Thermodynamic parameters

The values of the thermodynamic parameters calculated from the isotherms associated with the Pb (II) adsorption

processes at different temperatures are shown in Table 3, and they reflect the feasibility and the spontaneous nature of the process.

A value of $\Delta H = 10.62$ kJ/mol suggests an endothermic adsorption process, and ΔG shows a negative tendency indicating spontaneous adsorption. The magnitude of ΔH is related to the reaction mechanism. If ΔH has values lower than 84 kJ/mol, this corresponds to a physisorption process, and values between 84 and 420 kJ/mol correspond to a chemisorption process (Errais *et al.* 2011). The value obtained of 10.6 kJ/mol indicates that the predominant adsorption process is physical, and the value of $\Delta S = 0.0411$ kJ/mol indicates that the material could be regenerated.

Table 3 | Thermodynamic parameters of the adsorption of Pb (II) by AL-ZMR

Temperature (°C)	ΔG (kJ/mol)	ΔH (kJ/mol)	ΔS (kJ/mol)
25	–1.6		
40	–2.347	10.625	0.041
50	–2.602		

Column adsorption

The breakthrough curves obtained for the removal of Pb (II) by AL-ZMR at different initial concentrations of Pb (II) (10 and 30 mg/L) are shown in Figure 9. The most important parameters of the breakthrough curve (adsorption capacity (q_e) and the removal percentage) were determined at the time of saturation (t_{sat}), and they are shown in Table 4.

Table 4 shows the longest service time was observed in the columns where the initial concentration was 30 mg/L, and the saturation time was from 1,308 to 2,491 min when

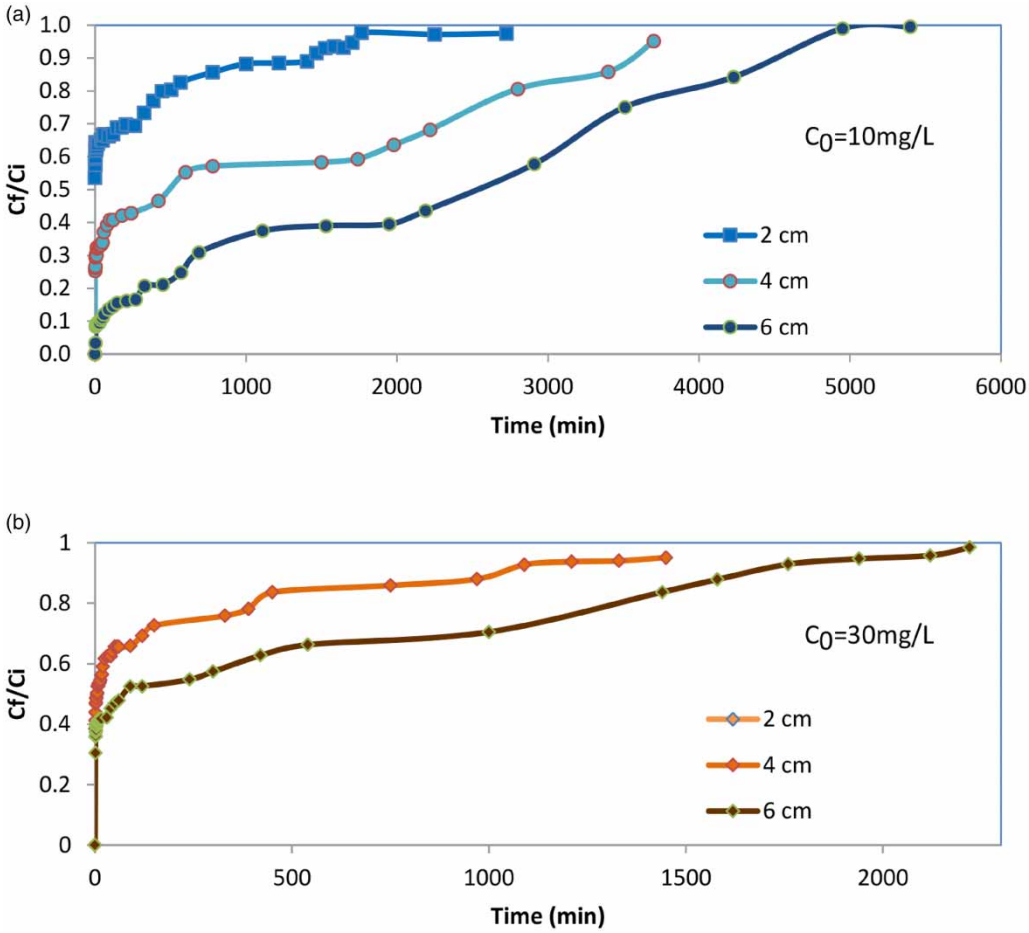

Figure 9 | Breakthrough curves for the adsorption of Pb (II) at $C_i = 10$ mg/L (a) and 30 mg/L (b).

Table 4 | Experimental parameters of the breakthrough curves for the adsorption of Pb (II)

Parameter	Pb (II) v (mL/min) = 3					
C_0 (mg/L)	10			30		
m (g) dry base	0.423	0.846	1.27	0.423	0.846	1.27
H (cm)	2	4	6	2	4	6
q_{total} (mg)	22.28	44.87	57.14	22.95	24.67	38.34
q_e (mg/g)	52.67	53.03	44.99	54.25	29.16	30.18
m_{total} (mg)	81.75	111	162	94.5	130.5	199.8
% removal	27.25	40.42	35.27	24.28	18.90	19.18
t_{sat} (min)	3,706	4,290	6,115	1,308	1,564	2,491
Z_m (cm)	1.99	3.52	3.53	1.99	3.98	5.81

m = adsorbent mass on dry base, H = bed height, t_{sat} = saturation time, Z_m = height of mass transfer zone.

the height increased from 2 to 6 cm and, on the other hand, the capacity of the columns increased; this could be attributed to the increase in the number of active sites in the bed due to the amount of packed material (Vijayaraghavan *et al.* 2006; Mishra *et al.* 2013).

The initial concentration of Pb (II) has a significant effect on the breakthrough curves, and the saturation time increases as the saturation decreases. This behavior can be explained by the fact that at a high concentration, the metal ions cover the sites of active sorption faster (Morosanu *et al.* 2017).

The values of the experimental parameters (Table 4) indicate that for saturation for $C_0 = 10$ mg/L and $H = 2$ cm the t_{sat} is 3,706 min, and this last value decreases to 1,308 when the concentration increases to 30 mg/L; for the lowest concentration of Pb (II) (10 mg/L) and $H = 4$ cm, the saturation is in 4,290 min, and for 30 mg/L the t_{sat} is 1,564 min. The same behavior was observed for the height of 6 cm.

With an increase of the feed concentration solution, the amount of metal ions increases, and a smaller volume of water can be treated before the sorption bed is saturated.

Regeneration of the adsorbent

Four successive adsorption–regeneration cycles were carried out and the AL-ZMR adsorbent maintained a similar adsorption percentage in each of the four cycles. There was only a slight decrease of 4% in the fourth cycle, compared with the first one. Figure 10 shows a comparison of the percentages of adsorption and desorption in the successive cycles.

On the other hand, the percentage of Pb (II) desorption decreased approximately 30% for the fourth cycle. This decrease may be due to a modification of the functional groups of the adsorbent that have more affinity for the metal, thus decreasing desorption of Pb (II) (Athar *et al.* 2013).

CONCLUSIONS

The micrographs of the AL-ZMR beads show the porosity and the rough surface of the material. The pH-zpc was 4.6

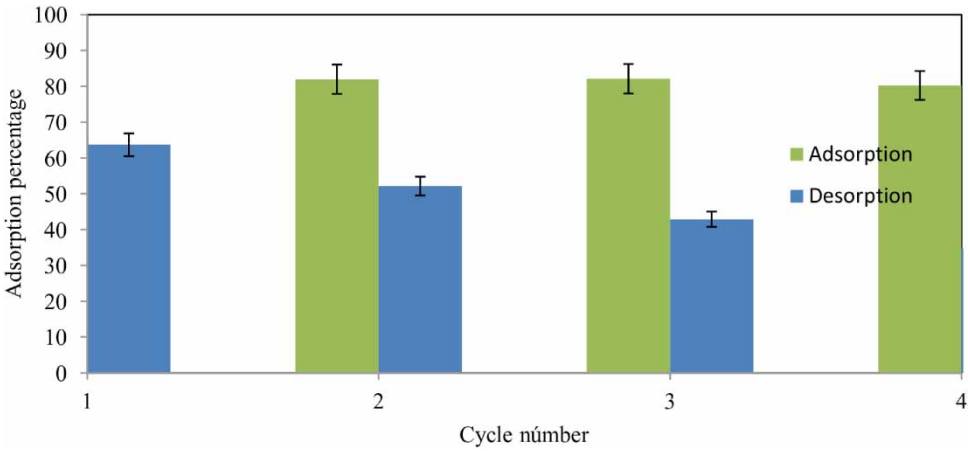

Figure 10 | Percentages of adsorption and desorption in four consecutive cycles.

and at this pH value the charge of the surface of beads is neutral. Below this pH the predominant surface charge is positive and above this value it is negative. The analysis of FTIR allowed the identification of the main functional groups of the AL-ZMR beads such as the hydroxyl and carboxyl groups, which are responsible for the removal of the Pb (II) ions from solution. A removal capacity of 2 mg/g was obtained for AL-ZMR at 25, 40 and 50 °C and equilibrium was reached in 60 min at 25 °C and in 30 min at 40 and 50 °C. The optimum pH for biosorption of Pb (II) was 5. The adsorption kinetics data were adjusted to the pseudo-second-order model. The Freundlich isotherm model better approximates the Pb (II) equilibrium data, suggesting that the surface of the adsorbent is heterogeneous. The enthalpy value (ΔH) of 10.6 kJ/mol shows that physical interaction of the process predominates. The thermodynamic parameters indicate that the process is spontaneous and endothermic. The initial concentration of Pb (II) has a significant effect on the breakthrough curves; as the concentration decreases, the saturation times increase.

ACKNOWLEDGEMENTS

The authors thank the Tecnológico Nacional de Mexico for the financial support project 6355.17-P and CONACYT for the grant to D. Gutierrez Lopez.

REFERENCES

Al-Anber, Z. A. & Al-Anber, M. A. S. 2008 Thermodynamics and kinetic studies of iron(III) adsorption by olive cake in a batch system. *J. Mex. Chem. Soc.* **52**, 108–115.

Almeida, C. A. P., Debacher, N. A., Downs, A. J., Cottet, L. & Mello, C. A. D. 2009 Removal of methylene blue from colored effluents by adsorption on montmorillonite clay. *J. Colloid Interface Sci.* **332**, 46–53.

Amaringo Villa, F. A. & Hormaza Anaguano, A. 2013 Determination of the point of zero charge and isoelectric point of two agricultural wastes and their application in the removal of colorants. *RIAA* **4**, 27–36.

Athar, M., Farooq, U., Aslam, M. & Salman, M. 2013 Adsorption of Pb(II) ions onto biomass from *Trifolium resupinatum*: equilibrium and kinetic studies. *Appl. Water Sci.* **3**, 665–672.

Cardona Gutiérrez, A. F., Cabañas Vargas, D. D. & Zepeda Pedreguera, A. 2013 Evaluación del poder biosorbente de cáscara de naranja para la eliminación de metales pesados, Pb(II) y Zn(II). *Rev. Ac. Ing., UADY* **17** (1), 1–9.

Carreño de León, M. C., Solache Ríos, M. J., Flores Alamo, N., Hernández Berriel, C. & Juárez Robles, O. 2016 Biosorption of lead (II) and chromium with *Zea mays* rachis in aqueous solutions: characterization studies. *Afinidad* **73** (574), 140–147.

Carreño de León, M. C., Flores Alamo, N., Solache Ríos, M. J., De la Rosa Gómez, I. & Díaz Campos, G. 2017 Lead and copper adsorption behaviour by *Lemna gibba*: kinetic and equilibrium studies. *CLEAN Soil Air Water* **45** (8), 1600357.

Chang, R. 2007 *Química*, 9th edn. McGraw Hill Interamericana S.A. de C.V., Mexico.

Chatterjee, A. & Schiewer, S. 2014 Multi-resistance kinetic models for biosorption of Cd by raw and immobilized citrus peels in batch and packed-bed columns. *J. Chem. Eng.* **244**, 105–116.

Errais, E., Duplay, J., Darragi, F., M'Rabet, I., Aubert, A., Huber, F. & Morvan, G. 2011 Efficient anionic dye adsorption on natural untreated clay: kinetic study and thermodynamic parameters. *Desalination* **275**, 74–81.

Febrianto, J., Kosasih, A. N., Sunarso, J., Ju, Y.-H., J., Indraswati, N. & Ismadji, S. 2009 Equilibrium and kinetic studies in adsorption of heavy metals using biosorbent: a summary of recent studies. *J. Hazard. Mater.* **162**, 616–645.

Foo, K. Y. & Hameed, B. H. 2010 Insights into the modeling of adsorption isotherm systems. *J. Chem. Eng.* **156**, 2–10.

García-Rosales, R. & Colín-Cruz, A. 2010 Biosorption of lead by maize (*Zea mays*) stalk sponge. *J. Environ. Manage.* **91** (11), 2079–2086.

Guyo, U., Mhonyera, J. & Moyo, M. 2015 Pb(II) adsorption from aqueous solutions by raw and treated biomass of maize stover – a comparative study. *Process Saf. Environ. Prot.* **93**, 192–200.

Hasan, S. H., Singh, K. K., Prakash, O., Talat, M. & Ho, Y. S. 2008 Removal of Cr(VI) from aqueous solutions using agricultural waste 'maize bran'. *J. Hazard. Mater.* **152**, 356–365.

Hernández-Hernández, H. K. A., Solache-Ríos, M. & Díaz-Nava, M. C. 2013 Removal of brilliant blue FCF from aqueous solutions using an unmodified and iron-modified bentonite and the thermodynamic parameters of the process. *Water Air Soil Pollut.* **224**, 1562.

Ho, Y. S. & McKay, G. 1998 Comparison of chemisorption kinetic models applied to pollutant removal on various sorbents. *Process Saf. Environ. Prot.* **76**, 332–340.

Juárez, O. 2014 *Removal of Lead and Chromium in Aqueous Samples Using Zea Mays Rachis*. MSc thesis, National Technological Institute of Mexico (Toluca), State of Mexico, Mexico.

Liu, Y., Sun, X. & Li, B. 2010 Adsorption of Hg^{2+} and Cd^{2+} by ethylenediamine modified peanut shells. *Carbohydr. Polym.* **81**, 335–339.Mahajan, G. & Sud, D. 2013 Application of ligno-cellulosic waste material for heavy metal ions removal from aqueous solution. *J. Environ. Chem. Eng.* **1**, 1020–1027.

Makeswari, M., Santhi, T. & Aswini, P. K. 2016 Adsorption of nickel ions by using binary metal oxides from aqueous solution. *Int. J. Adv. Res.* **4** (2), 542–553.

Mishra, V., Balomajumder, C. & Agarwal, V. K. 2013 Adsorption of Cu (II) on the surface of nonconventional biomass: a study on forced convective mass transfer in packed bed column. *J. Waste Manage.* **2013**, 632163.

Morosanu, I., Teodosiu, C., Paduraru, C., Ibanescu, D. & Tofan, L. 2017 Biosorption of lead ions from aqueous effluents by rapeseed biomass. *New Biotechnol.* **39**, 110–124.

Moyo, M., Chikazaza, L., Nyamunda, B. C. & Guyo, U. 2013 Adsorption batch studies on the removal of Pb(II) using maize tassel based activated carbon. *J. Chem.* **2013**, 508934.

Park, D., Lim, S.-R., Yun, Y.-S. & Park, J. M. 2008 Development of a new Cr(VI)-biosorbent from agricultural biowaste. *J. Bioresour. Technol.* **99**, 8810–8818.

Petrović, M., Šoštarić, T., Stojanović, M., Milojković, J., Mihajlović, M., Stanojević, M. & Stanković, S. 2016 Removal of Pb^{2+} ions by raw corn silk (*Zea mays* L.) as a novel biosorbent. *J. Taiwan Inst. Chem. Eng.* **58**, 407–416.

Pinzón-Bedoya, M. L. & Vera Villamizar, L. E. 2009 Kinetic modeling biosorption of Cr (III) using orange shell. *Dyna* **76**, 95–106.

Ren, H., Gao, Z., Wu, D., Jiang, J., Sun, Y. & Luo, C. 2016 Efficient Pb(II) removal using sodium alginate–carboxymethyl cellulose gel beads: preparation, characterization, and adsorption mechanism. *Carbohydr. Polym.* **137**, 402–409.

Roulia, M. & Vassiliadis, A. A. 2008 Sorption characterization of a cationic dye retained by clays and perlite. *Microporous Mesoporous Mater.* **116**, 732–740.

Sankararamakrishnan, N., Kumar, P. & Singh Chauhan, V. 2008 Modeling fixed bed column for cadmium removal from electroplating wastewater. *Separ. Purif. Technol.* **63**, 213–219.

Tan, G., Yuan, H., Liu, Y. & Xiao, D. 2010 Removal of lead from aqueous solution with native and chemical modified corncobs. *J. Hazard. Mater.* **174**, 740–745.

Vijayalakshmi, K., Mahalakshmi Devi, B., Latha, S., Gomathi, T., Sudha, P. N., Venkatesan, J. & Anil, S. 2017 Batch adsorption and desorption studies on the removal of lead (II) from aqueous solution using nanochitosan/sodium alginate/microcrystalline cellulose beads. *Int. J. Biol. Macromol.* **104**, 1483–1494.

Vijayaraghavan, K., Padmesh, T. V. N., Palanivelu, K. & Velan, M. 2006 Biosorption of nickel(II) ions onto *Sargassum wightii*: application of two-parameter and three-parameter isotherm models. *J. Hazard. Mater.* **133**, 304–308.

Vilchis, G. J. 2013 *Adsorption of Pb(II) Present in Aqueous Solution onto Calcium, Strontium and Barium Hydroxyapatites*. Master's thesis, Faculty of Chemistry, Universidad Autonoma del Estado de Mexico, Toluca, Mexico State, Mexico.

Wang, J. & Chen, C. 2009 Biosorbents for heavy metals removal and their future. *Biotechnol. Adv.* **27**, 195–226.

Worch, E. 2012 *Adsorption Technology in Water Treatment: Fundamentals, Processes, and Modeling*. Walter de Gruyter GmbH and Co. KG, Berlin, Germany.

First received 16 October 2019; accepted in revised form 13 May 2020. Available online 25 May 2020